Improved performances and capabilities of the Cooled Mid-Infrared Camera and Spectrometer (COMICS) for the Subaru Telescope

Yoshiko K. Okamoto[a], Hirokazu Kataza[b], Takuya Yamashita[c], Takashi Miyata[d], Shigeyuki Sako[d], Shin-ya Takubo[d], Mitsuhiko Honda[d], and Takashi Onaka[d]

[a] Institute of Physics, Center for Natural Science, Kitasato University, 1-15-1 Kitasato, Sagamihara, Kanagawa 228-8555, Japan;

[b] Institute of Space and Astronautical Science, Sagamihara 229-8510 Japan;

[c] Subaru Telescope, NAOJ, 650 North A'ohoku Pl., Hilo HI96720, U.S.A.;

[d] University of Tokyo, Bunkyo-ku, Tokyo 113-0033, Japan;

ABSTRACT

COMICS is an observatory mid-infrared instrument for the 8.2 m Subaru Telescope. It is designed for imaging and spectroscopic observations in the N- (8-13 micron) and Q-bands (16-25 micron) atmospheric windows. The design and very preliminary performances at the first light observations in December 1999 were reported at the SPIE meeting in 2000. We describe here the improved performances of COMICS and capability of high spectral resolution spectrocopy which became available from December 2001. We will also briefly report prelimnary scientific results.

Keywords: Mid-Infrared, Ground-based instrument, Spectrometer, Camera, Subaru Telescope

1. INTRODUCTION

COMICS is an observatory mid-infrared instrument for the 8.2 m Subaru Telescope[1] at Mauna Kea. It is designed for imaging and spectroscopic observations in the N- (8-13 micron) and Q-band (16-25 micron) atmospheric windows. It achieved the first light observations December 1999. The design and very preliminary performances were reported at the SPIE meeting in 2000[2]. From the data of test observations made after the first light, reliable performance characteristics of COMICS have been evaluated, such as sensitivity, observing efficiency, stability of the instrument, and spatial resolution in short and long time integrations.

Also continuous improvements bring many new observing capabilities. Especially, all of the six detector arrays planned were installed in COMICS November 2001 for the first time. Thanks to this progress, we tested N-band medium-resolution spectroscopy by using all of the five spectroscopic detector arrays and confirmed that two exposure sets of the grating position can cover the whole N-band spectra. This provides a great merit when one makes medium-resolution (R∼2500) spectroscopy in terms of the high observing efficiency. Also thanks to a new narrow-band filter for [NeII] 12.8 micron wavelength, high resolution spectroscopy(R∼10000) became available and was tested. These high resolution spectroscopic observing modes were confirmed to have a much higher sensitivity in the detection of line emissions than low-resolution spectroscopy mode (R=250). During these two years, control computers and readout electronics were replaced to improve the data readout speed and increase the observing efficiency. Appropriate methods of the observations and data reduction were developed based on the actual observed data. Due to these results, COMICS was opened for common use from July 2002.

In this paper, we summarize the current performances and improvements so far made (§ 2, 3, and 4) and also report some prelimnary scientific results (§ 5).

Y. K. O. : E-mail: okamtoys@cc.nao.ac.jp, Telephone 81 42 778 8034.
S. T. : Present address: Nikon Corporation, Japan.

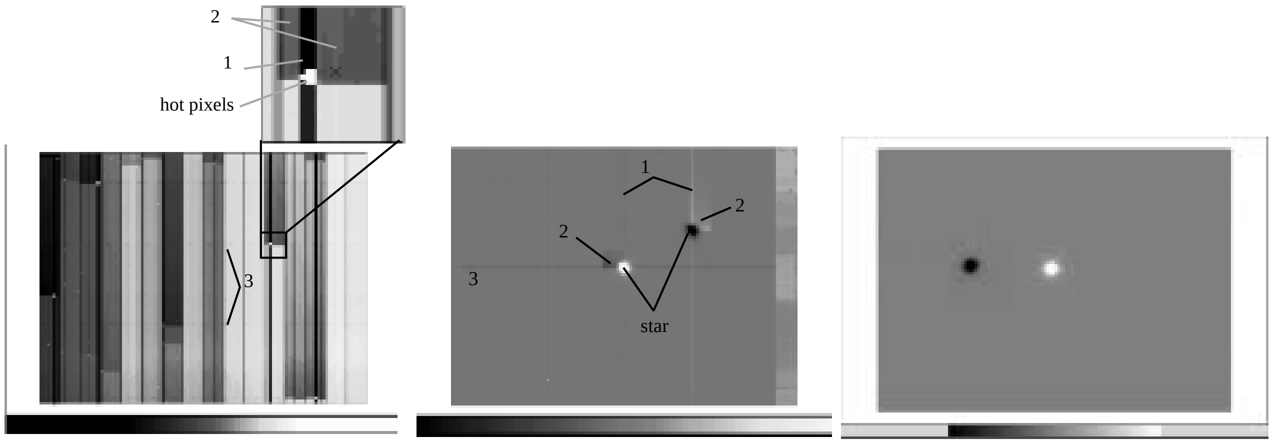

Figure 1. Drooping phenomena before and improving detector readout method (*Right two panels*). Level shifts along columns, level shifts within the same channel, and drop of zero level are denoted with 1, 2, and 3, respectively. (*Left*) Dark image with magnified show around hot pixels. (*Center*) Standard star image frame after chop subtraction. On- and off-beam stellar image is shown with drooping phenomena. (*Right*) Standard star image after improvement of detector read out method.

2. IMPROVEMENT AND CURRENT STATUS

2.1. Detectors

COMICS was designed to employ five Raytheon 320x240 Si:As IBC detector arrays for the spectroscopy to obtain whole N-band spectra with R$\sim$2500 efficiently. November 2001, all of the five detectors were installed into the COMICS dewar. Now one can obtain the whole R$\sim$2500 spectra in the N-band with only two grating configurations. Imaging mode was designed to employ one detector array and the array has been installed from the first light observations.

2.1.1. Drooping Effects

At the first light observations, it was found that the detector arrays used for COMICS showed 'drooping effects': that is a phenomenon that the pixel output values become non-linear and/or are affected by their surrounding pixels when strong light enters[3]. Thie effect is different from cross talks between pixels. A similar phenomenon was reported for the detectors of SIRTF/IRC [*]. In the case of the detectors of COMICS, the drooping effects are classified into three types as shown in Figure 1.

- The first is output level shifts along columns of detectors. When a certain column was examined, the count of the pixels after a pixel where a high count had been read out decreased compared to those for the pixels before the pixel of high count. This phenomenon is triggered by hot pixels and bright objects. The maximum shift values are independent of the height of the high count and are almost constant (r.m.s.$\sim$230ADU for the spectroscopic detector 1) except for completely saturated hot pixels.
- When the level shifts along columns are large, they affect the columns in the same channel and cause the second type drooping effect: the level shifts within channels. The counts of pixels read out after the high count pixel drop down (these pixels must belong to the same channel of the high count pixel).
- The third is a drop of zero level, appearing for all pixels of the same rows of the whole detector. Their shift values are estimated to be constant along rows in most cases. This is caused by a group of high count pixels, such as a group of hot pixels, an image of bright objects, and a bright spectrum.

[*]Van Cleve, J. at NGST Detector Workshop, April 1999.
See http://www.ngst.stsci.edu/conferences/detector_conf99/detector_conf.html

All of these level shifts were caused by a drop of reset level of detector readout oultiplexers. The readout method was improved to read all of the reset levels as well as the signal levels, then the drooping problem was solved[4].

2.2. Filters

At the first light observations, only basic filters for imaging and spectrosopy of R≤2500 were available. We joined the VISIR filter consortium and added some specific filters, whose wavelength coverage was adjusted to some band or line features. Especially, some narrow band filters were prepared to avoid mixing of fluxes of different orders for R∼10000 spectroscopy . Currently availble filters are summarized in Table 2.2.

Table 1. Newly available filters which are not listed in the last report[2]. Note that for the fore-optics filter wheels, only 9 filters can be installed at the same time and for the imaging filter wheel, only 10 filters can be installed at the same time. These numbers do not include the dark filters and blank filters. The filters which will be available in a year are indicated by dagger.

ID	Wavelength[μm]		Name	Diameter	Manufacturer
	Center	Width			
Fore-optics filters					
02	18.75	4.7	Q short	40mm	ORT
22	8.6	0.43	PAH1	1.5”	OCLI
29	11.3	0.6	PAH2	1.5”	Reading
30	12.81	0.2	NeII	1.5”	Reading
34	17.0	0.4	QH2	1.5”	Reading
23	8.99	0.13	ArIII	1.5”	OCLI
26	10.52	0.16	SIV	1.5”	OCLI
31†	13.1	0.2	NeII ref.	1.5”	Reading
Imaging filters					
11	24.5	2.2	Q24.5	1”	Reading
33	16.5	0.4	Q0	1”	Reading
35	17.0	0.4	QH2	1”	Reading
36	17.65	0.9	Q1	1”	Reading
37	18.75	0.85	Q2	1”	Reading
48	16.5	0.4	Q0	1”	Reading
24†	9.2	0.14	ArIII ref.	1”	OCLI
32†	13.1	0.2	NeII ref.	1”	Reading
38†	19.5	0.4	Q3	1”	Reading
39†	20.5	1.0	Q4	1”	Reading
42†	24.5	0.8	Q8	1”	Reading

2.3. Observing Efficiencies

Current performances are summarized in § 3. During the test observations, low observing efficiencies and frequent excess noises which especially occurred under long integration for R∼2500 spectroscopy were serious problems. The observing efficiencies were low due to slow data transfer from the frame memory controller boards to the data storing hard disk drives. In addition, imaging observations suffer also from the electronic ND filters, which discard part of the integration time without integrating the signals. To solve these problems, the control computer of the VME-bus workstation was replaced by a Linux PC and the partial readout method for imaging was developed. Details of these improvement are described by Sako et al. in this volume and we just summarize the improved observing efficiencies in the next section. The large noise problem will be solved by replacing the A/D convertor boards.

2.4. Newly Capabilities Tested

At the first light observations, the imaging and the R∼250 spectroscopy were tested. After installing all of the five spectroscopic detector arrays, the R∼2500 spectroscopy using all of the arrays was tested. The example of the spectral data obtained with the five arrays and two grating configurations are shown in Figure 2. Between the two exposure sets, the grating angle was adjusted and the wavelength coverage of the second exposure covered the wavelengths, which had not been observed in the first exposure.

The narrow band filter at 12.8μm was installed September 2001 and the R∼10000 spectroscopy was tested at the filter wavelengths. The obtained [NeII] line frame toward an ultracompact HII region G111.61+0.37 is shown in Figure 3. The central wavelength of the line changes along the slit and we detected the line velocity variation of 10 km/s.

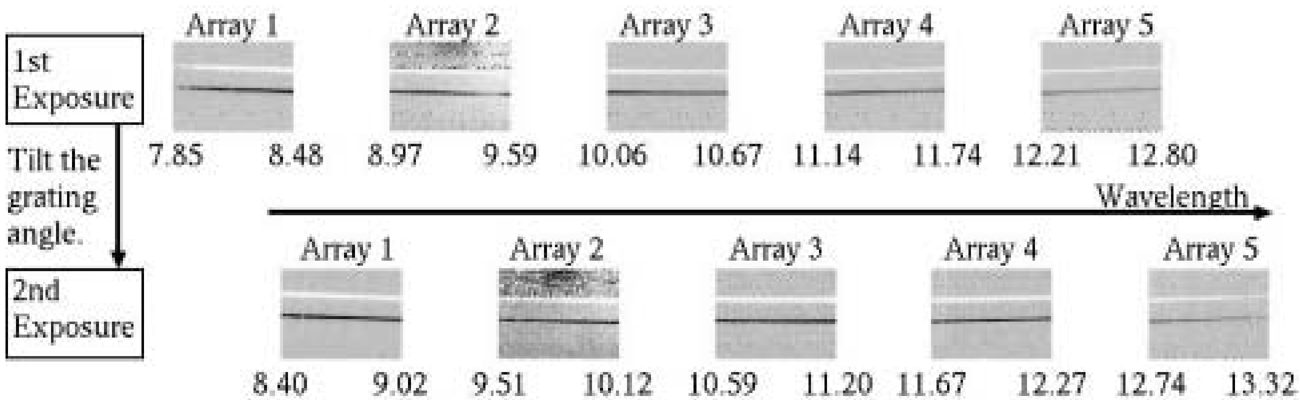

Figure 2. Spectral data of a standard star obtained with five spectroscopic arrays. Top five frames show the data obtained with the first grating setting and the bottom frames show those with the second grating setting after changing the grating angle. Shown frames are after chop subtraction and the white curves shows the on-beam (plus) star spectra and the black curves shows the off-beam (minus) star spectra.

3. CURRENT PERFORMANCES

3.1. Sensitivity

The sensitivity for 5σ in 30 minutes integration is listed in Table 3.1 and shown in Figure 4. The values are for the observations with only chopping without nodding. The primary mirror nodding reduces the described sensitivity by a factor of $\sqrt{2}$ compared to the staring observation, because the noise is increased when subtracting the frames.

3.2. Spatial Resolutions

The diffraction limited resolutions have been achieved all of the observing modes of the COMICS. However, due to tracking and guiding errors of the telescope, the spatial resolution of the total system is degraded down to 0.5" for the integration longer than 50msec. Two data taking modes are prepared, ADD and RAW, where every frame is saved to disk in the RAW mode and the frames are co-added for every chop beam movement before being saved in the ADD mode. To avoid the degradation, the shift-and-add method can be used for bright objects with the RAW modes. The degradation is not significant for the Q-band observations.

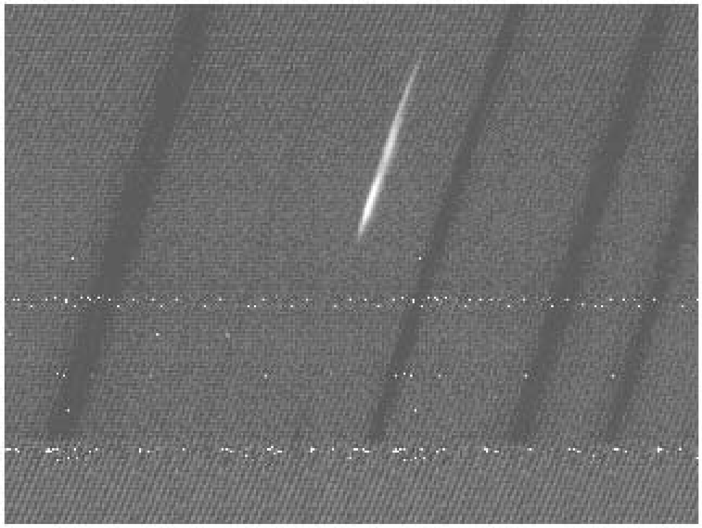

Figure 3. R∼10000 spectral image frame of [NeII] emission toward G111.61+0.37. The horizontal axis corresponds to the dispersion direction. The white tilted line is the detected [NeII] line emission and black tilted broad lines are atmospheric emission lines remaining even after the chopped image subtraction.

Table 2. Sensitivity values (5σ 30min) for COMICS imaging.

Wavelength[μm]		Sensitivity	
Center	Width	Point Sources [mJy]	Diffuse Sources [mJy/arcsec^2]
8.8	0.8	7.9	50
9.7	0.9	4.8	38
10.5	1.0	6.8	65
11.7	1.0	3.0	35
12.4	1.2	6.5	80
18.5	1.2	33	640
20.8	0.9	97	1250
24.5	2.2	45	930

3.3. Spectral Resolutions

Spectral resolutions were measured by ionic line emissions from massive star forming regions. They are listed in Table 3 and shown in Figure 5. For the resolution of R∼10000 spectroscopy, the line emissions toward G111.61+0.37 were likely to be intrinsically broader than the instrumental resolution and only lower limits were derived.

3.4. Observing Efficiencies

The observing efficiency is defined as the ratio of the integration time to the net observing time including the transfer time of data files and the loading time of detector reading out clocks. Here, the efficiencies assume that 4 chop/nod frames include the target. For extended targets (larger than ∼15") where the target cannot be placed on all 4 frames, the efficiency will be 4 times lower. The values do not include the overhead for the object acquisition and standard star observations.

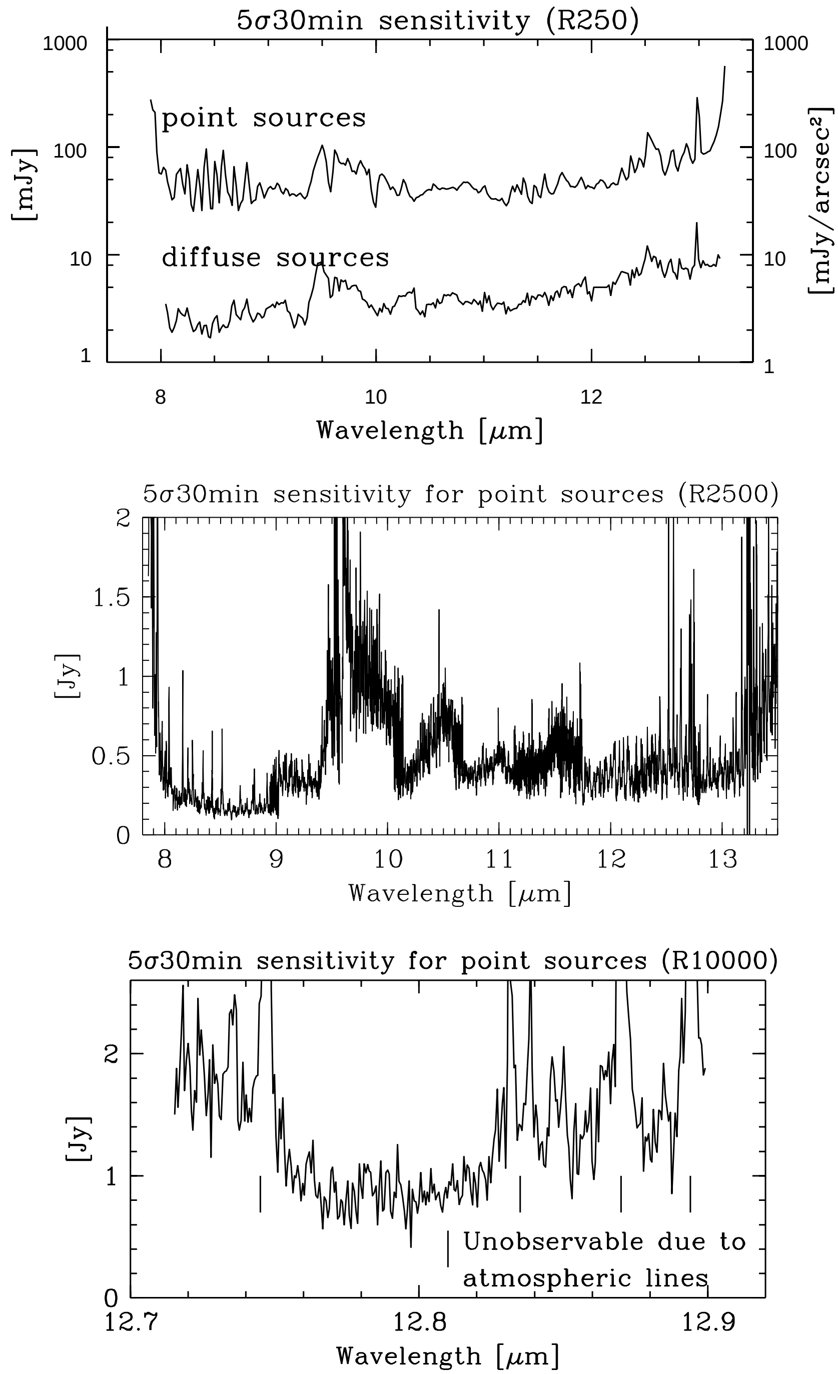

Figure 4. 5σ 30min sensitivity of R∼250–10000 spectroscopy.

Table 3.

Wavelength [μm]	Spectral Resolution	Line
R∼250 spectroscopy		
8.99	180	[ArIII]
10.51	240	[SIV]
12.81	270	[NeII]
R∼2500 spectroscopy		
8.99	2600	[ArIII]
12.81	3100	[NeII]
R∼10000 spectroscopy		
12.81	>8500	[NeII]

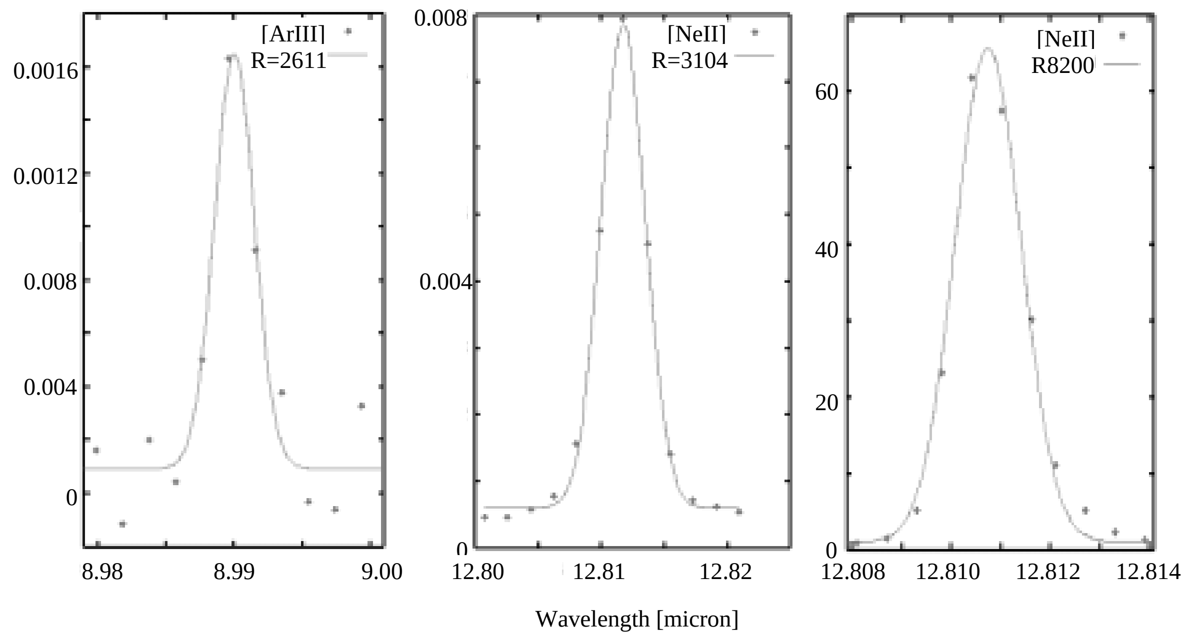

Figure 5. Demonstration of the spectral resolutions of COMICS. (*Left two panels* [ArIII] 8.99μm line and [NeII] 12.81μm line toward G111.61+0.37 obtained with R∼2500 spectroscopy. *Rightmost panel* [NeII] 12.81μm toward the same object obtained with R∼2500 spectroscopy.

Before the replacement of the control computer, the observing efficiency was 3.6-16% for RAW mode imaging. The current efficiencies after the replacement listed in Table 4 are improved by a factor of 2–3.

For the imaging observations, the maximum exposure time may be less than the readout time due to the high background. However, the shortest exposure time is determined by the readout electronics. To avoide saturation of the pixels, elctronic ND filters are used to discard part of the exposure time as non-integrating time. This method makes the observing efficiency fairly low. This can be overcome by reading part of the array to reduce the readout time (all 320 columns must always be read). Table 4 also lists the maximum number of the rows which can be read without the electronic ND filters. For the N-band, this problem will be solved by the newly manufactured A/D convertor boards which enable 1.7 times faster exposure time and the efficiencies will be improved up to 64% in the ADD mode and 44% in the RAW mode.

Furthermore, since the chopping profile is not a perfect square wave, the exposure frames just after the chopping must be discarded due to the unstationary telescope position. This causes the loss of the observing time especially in the imaging mode, where chopping frequecy is high.

Table 4. Observing efficiencies for imaging observations.

Filter	N8.8	N9.7	N10.5	N11.7	N12.4	Q18.5	Q20.8	Q24.5
ADD mode	64%	24%	32%	48%	24%	8%	28%	8%
RAW mode	44%	16%	22%	32%	16%	6%	18%	6%
Max Width	240	90	120	180	90	30	100	30

Table 5. Observing efficiencies for spectroscopic observations in the N-band.

Resolution	R250	R2500	R10000
ADD mode	68%	80%	88%
RAW mode	56%	-	-

The observing efficiency for spectroscopic observations are listed in Table 5. Here, the efficiencies assume that all of the chop/nod positions are on-source. For extended targets (larger than ∼15”) where the target cannot be placed on the array for all 4 frames, the efficiency will be 4 (2) times lower for R250 (R2500 and R1000) spectroscopy. (For R2500 and R10000 spectroscopy, the nodding is not required for background subtraction.)

3.5. Stability of the Instrument

3.5.1. Reproductivity of Moving Parts

The reproductivity of the slit image after rotating the slit wheel is better than 0.2 pixel on the imaging detector. That after rotating the lens wheel is better than 0.1 pixel. The reproductivity of the filters are estimated as high as that of the slits because the filter wheels have the same structure as the slit wheel.

The grating has less positional reproductivity in both of switching and changing the angle. When the grating was changed, the slit image position on the spectroscopic detectors fluctuates within several pixels. That of returning to the same angle after rotating the grating box amounts to several to 10 pixels on the spectroscopic detectors. One should take flat frames for object frames without switching and changing the grating angle.

3.5.2. Rigidity of the Optical Structure

Flexure of the optical system comes from distortion of the cold base plate and each optical unit. They are dependent on the elevation angle and instrument rotator angle. The total flexure is measured by the slit image position on the detectors at four position angles of the instrument rotator (PAIR=0, 90, 180, 270°) and five elevation angles (El=30, 45, 60, 80, 90°). The results are shown in Figure 6. The flexure according to the elevation angle is negligible for PAIR=0 and 180°, and is less than 0.6 pixel for PAIR=±90° in the imaging. That for the spectroscopy is less than 1 pixel for PAIR=0 and -90° but amounts to 3 pixels at PAIR=90 and 180°. This large flexure causes the shift of the optical alignment in the object frames, calibration star frames, and flat frames. It can be corrected at the reduction procedure for the low-resolution spectroscopy. However, in the intermediate-resolution spectroscopy, the sensitivity fringe patterns[2] vary according to the elevation angle and to the PAIRs because of the different flexure. If one takes flat frames at different elevation angles and PAIRs from those of object frames, flat-fielding cannot be done accurately. To avoid this problem, one should take flat frames for the object frames at the same elevation angle and PAIRs as the object frames. The same method should be taken for the calibration star frames and their flat frames.

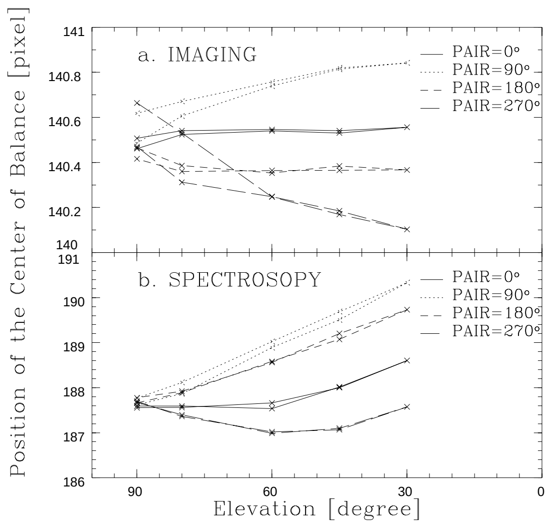

Figure 6. Flexure of the optics at different position angles of the instrument rotator (PAIRs) and elevations. Crosses denote the measured center of the slit images along a certain column on the imaging detectors. Though the deviation of the center is less than one pixel in the imaging, that in the spectroscopy amounts to one to three pixels.

4. OBSERVING METHOD AND DATA REDUCTION

4.1. Chop and Nod

Mid-infrared observations use 'chop and nod' technique to cancel out the background radiation. Chopping cancels the background emission which varies in a short time scale. Nodding cancels a pattern remaining in the subtracted frame made from two chopped beams. In the case of COMICS on the Subaru Telescope, the remaining pattern is negligible for bright objects. The threshold brightness is 5e-18 W cm^{-2} μm^{-1} arcsec^{-2} ($\sim$8 Jy/arcsec^2). Only the secondary chop is needed for the observations of such objects.

4.2. Chopping Frequencies Required to Reduce the Background Emission

The chopping frequency must be faster than a certain frequency in order to suppress the excess noise due to the background fluctuation over the shot noises. The cutoff frequency for the imaging is 0.7 Hz at 7.8 and 8.8μm, 3 Hz at 10.5μm, and 10 Hz at 9.7 to 12.4 μm. That for the low-resolution spectroscopy is 0.5 Hz at the atmospheric H_2O emission lines and 0.1 Hz at the other wavelengths. For intermediate-resolution spectroscopy, 0.03 Hz and 0.02 Hz are the cutoff frequencies at the atmospheric H_2O emission lines and the others, respectively.

4.3. Flat Fielding

For the imaging data, self-sky flat is used for flat fielding. For R$\sim$250 spectra, we use thermal emission spectra of the wall of the telescope dome as flat frames taken at the end of the observing night. For spectroscopic data of R$\geq$2500, we close the cell cover and take its thermal emission spectra as flat frames. There is a slight variation in the pixel-wavelength relation with telescope position. When combined with large fringes in the sensitivity, this requires precise flatfield frames to be taken at the same elevation and grating setting before slewing the telesocpe in order to properly calibrate R$\geq$2500 spectroscopic data.

4.4. Wavelength Calibration

In the spectroscopy, the wavelength calibration can be made with the atmospheric emission lines. From the object spectra frames, the object frame is first subtracted by the dark current frame and divided by the flat frame to obtain sky spectrum. In the low-resolution spectroscopy in the N-band, about 40 atmospheric emission lines are observed in the sky spectra (Figure 7). By taking the correlation of peak positions of the atmospheric lines between the model[5] and the data, pixel-wavelength relations are obtained. The accuracy of the wavelength calibration is better than 0.0025μm (0.13 pixel). The same method can be used for R$\sim$2500 and R$\sim$10000 spectroscopy (Figures 9 and 8). For the former, much more emission lines are observable than the R$\sim$250 spectroscopy (Figure 9).

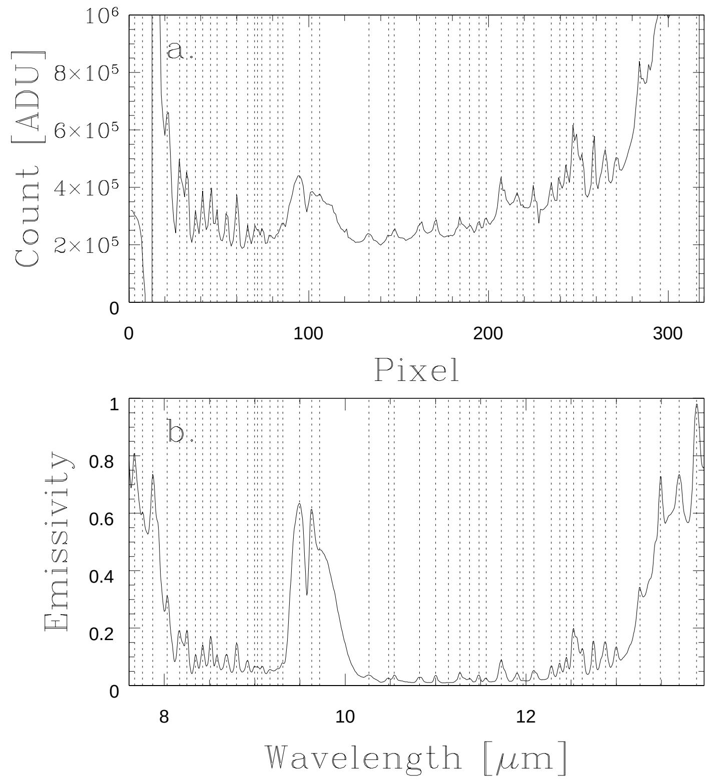

Figure 7. Comparison of the observed sky spectrum (*top*) and the model of the atmospheric emissivity (*bottom*) with the spectral resolution of 250. Dotted lines indicate the wavelength of the atmospheric emission lines.

4.5. Spatial Distortion

The spectrum of a point like source draws a curve on the detectors due to the image distortion in the camera optics. This distortion is described by two order polynomials approximately. When investigating a spatial variation in diffuse object spectra, the distortion must be corrected with that of calibration star spectra observed at the same PAIR as the object.

5. PRELIMINARY SCIENTIFIC RESULTS

The COMICS has unique characteristics of the high spatial resolution and high sensitivity for point sources. Mid-infrared observations with high spatial resolution are very important for probing massive star formation in detail. From our preliminary scientific results, we introduce the observations of ionics lines toward an ulracompact HII region K3-50A. The high resolution [NeII] map reconstructed from the observed spectra (Figure 10) obtained with the COMICS spectroscopy successfully resolves at least two central ionizing stars. This result indicates that K3-50A ultracompact HII region is ionized by a massive stellar cluster[5].

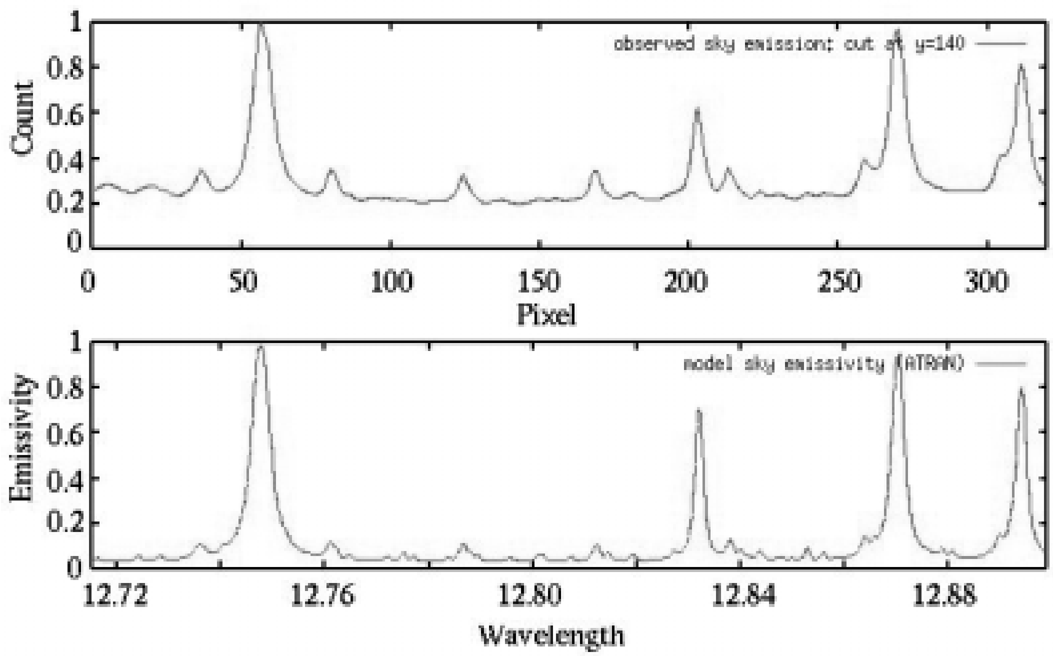

Figure 8. Comparison of the observed sky spectrum (*top*) and the model of the atmospheric emissivity (*bottom*) with the spectral resolution of 2500.

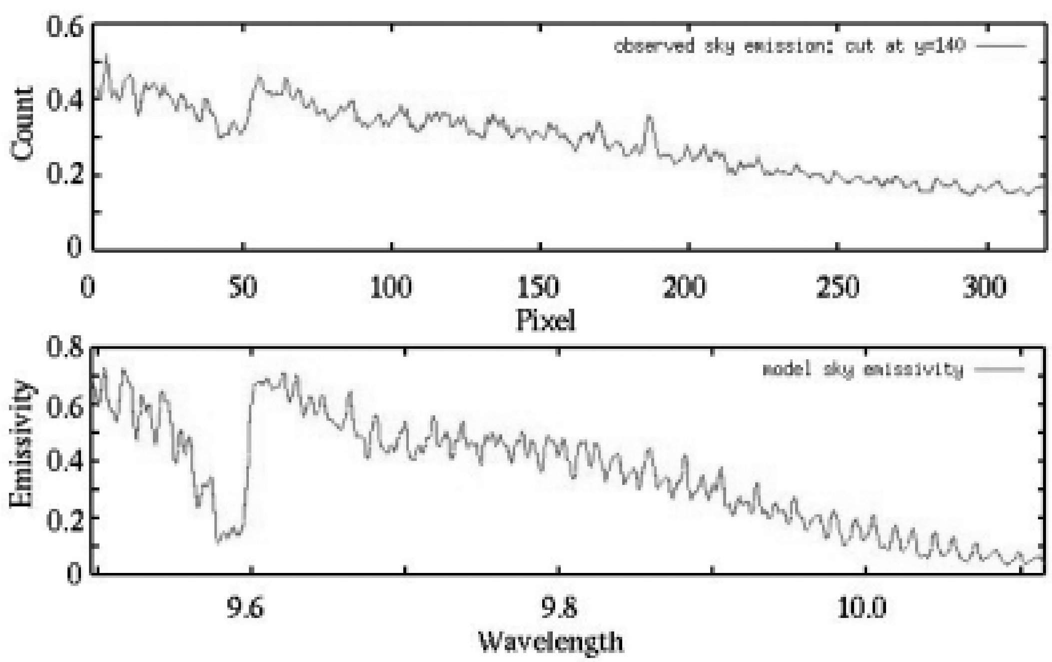

Figure 9. Comparison of the observed sky spectrum (*top*) and the model of the atmospheric emissivity (*bottom*) with the spectral resolution of 10000.

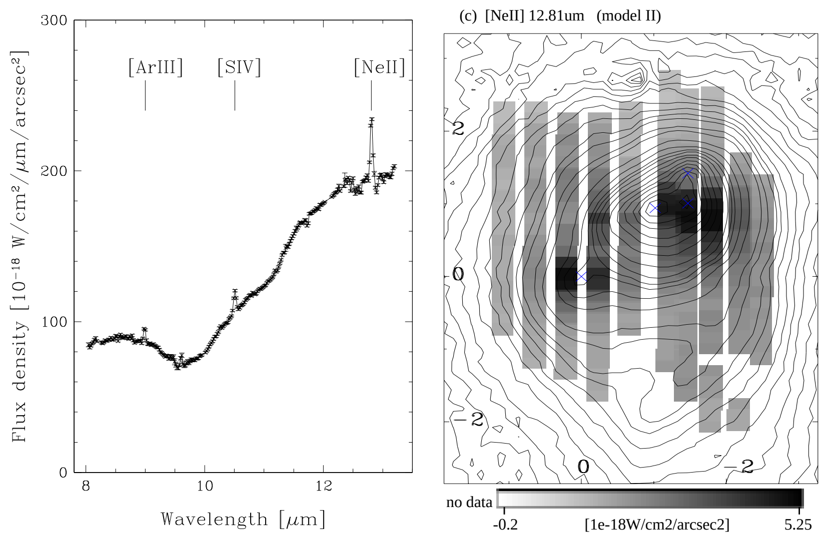

Figure 10. (*Left*) Sample R∼250 spectra toward K3-50A ultracompact HII region. (*Right*) Central [NeII] emission toward K3-50A reconstructed from slit-scanned R∼250 spectroscopy (greyscale) on 11.7μm image (contours).

ACKNOWLEDGMENTS

We wish to thank the support of the Subaru Telescope staff the during development and observations of COMICS. We are grateful to K. Nakamura for her contribution to the developpment of COMICS control software.

REFERENCES

1. Kaifu, N. et al. "The First Light of the Subaru Telescope: A New Infrared Image of the Orion Nebulae", *Publ. Astron. Soc. Japan*, **52**, p.1, 2000

2. Kataza, H., Okamoto, Y., Takubo, S., Onaka, T., Sako, S., Nakamura, K., Miyata, T., and Yamashita, T., "COMICS: The Cooled Mid-Infrared Camera and Spectrometer for the Subaru Telescope", *Proc. of SPIE* **4008**, p.1144, 2000

3. Okamoto, Y., "COMICS: A Mid-Infrared Camera and Spectrometer for the Subaru Telescope and Mid-Infrared Observations of Ultracompact HII Regions", *Dr thesis of Univ. of Tokyo, Japan*, 2001 4. Sako, S., "Improvement of read out method of COMICS detectors and Spectroscopic Observations of H_2 pure rotational emission lines from protostar disks", *Master thesis of University of Tokyo*, 2001

5. Lord, S. D. 1992, *A New Software Tool for Computing Earth's Atmospheric Transmission of Near- and Far-Infrared Radiation*, NASA